# Impact of phonons on dephasing of individual excitons in deterministic quantum dot microlenses

T. Jakubczyk,[1,2,*] V. Delmonte,[1,2] S. Fischbach,[3] D. Wigger,[4,†] D. E. Reiter,[4] Q. Mermillod,[1,2] P. Schnauber,[3] A. Kaganskiy,[3] J.-H. Schulze,[3] A. Strittmatter,[3] S. Rodt,[3] W. Langbein,[5] T. Kuhn,[4] S. Reitzenstein,[3,‡] and J. Kasprzak[1,2,§]

[1] *Univ. Grenoble Alpes, F-38000 Grenoble, France*
[2] *CNRS, Institut Néel, "Nanophysique et semiconducteurs" group, F-38000 Grenoble, France*
[3] *Institut für Festkörperphysik, Technische Universität Berlin, Hardenbergstraße 36, D-10623 Berlin, Germany*
[4] *Institut für Festkörpertheorie, Universität Münster, 48149 Münster, Germany*
[5] *Cardiff University School of Physics and Astronomy, The Parade, Cardiff CF24 3AA, United Kingdom*

Optimized light-matter coupling in semiconductor nanostructures is a key to understand their optical properties and can be enabled by advanced fabrication techniques. Using in-situ electron beam lithography combined with a low-temperature cathodoluminescence imaging, we deterministically fabricate microlenses above selected InAs quantum dots (QDs) achieving their efficient coupling to the external light field. This enables to perform four-wave mixing micro-spectroscopy of single QD excitons, revealing the exciton population and coherence dynamics. We infer the temperature dependence of the dephasing in order to address the impact of phonons on the decoherence of confined excitons. The loss of the coherence over the first picoseconds is associated with the emission of a phonon wave packet, also governing the phonon background in photoluminescence (PL) spectra. Using theory based on the independent boson model, we consistently explain the initial coherence decay, the zero-phonon line fraction, and the lineshape of the phonon-assisted PL using realistic quantum dot geometries.

Owing to the progress in the semiconductor growth, the self-assembled quantum dots (QDs) offer nowadays optimal quality of the residing exciton transitions [1] with enhanced emission efficiency [2–4] and close to ideal quantum optical properties [5]. Forthcoming applications emerging from combining QDs and nanophotonics – such as, quantum light sources in on-chip photonic networks – call for scalability and deterministic QD positioning. In this regard, in-situ electron beam lithography [6, 7] (EBL) has evolved into a suited technique for the deterministic fabrication of quantum light sources [8, 9]. When combined with a low temperature cathodoluminescence imaging, EBL permits to sculpture microlenses above individual QDs, enhancing collection efficiency over a broad spectral range.

Here, using four-wave mixing (FWM) micro-spectroscopy we reveal coherences of *single* QDs, deterministically embedded in microlenses realized by EBL. The resulting optical signals in these nanophotonic structures exhibit an enhanced signal to noise ratio. This enables us to infer the impact of acoustic phonons on the coherence dynamics of individual QDs. In particular, we report on the exciton zero phonon line (ZPL) dephasing close to the radiative limit in a single QD at 5 K, distinguishing it from its spectral wandering. Phonons are known to play a crucial role in the optical control of QDs [10, 11]. With increasing temperature, we observe an increasing impact of phonon-induced dephasing [12] owing to the polaron formation and wave packet emission [13, 14] and a broadening of the homogenous width $\gamma$, attributed to a quadratic coupling between carriers and acoustic phonons [16, 17]. Single QD micro-spectroscopy permits to associate the measured dephasing during the polaron formation with the spectral shape of phonon-assisted transitions, here accessed via photoluminescence (PL). We thus go beyond the FWM experiments performed on QD ensembles [1, 12], and we consistently explain the initial FWM decay, the zero-phonon line (ZPL) fraction, and the lineshape of the phonon-assisted PL using realistic QD geometry. Additionally, the optical parameters of QDs - i.e. dephasing, lifetime, dipole moments, phonon coupling - are to some extent averaged in QD ensemble measurement due to stochastic distribution of their shapes and alloy composition. This issue is naturally overcome in a single QD spectroscopy carried out here.

When performing FWM on single emitters on a simple planar structure one is confronted with a huge ratio between the resonant background (typically $10^6 - 10^8$ in the field, and $10^5$ when assisted with high quality anti-reflection coatings [18]) and the induced FWM. We have recently shown that, using suitable photonic nanostructures [19, 20], one can boost the experimental sensitivity by bringing a large amount of the field amplitude to the vicinity of a QD. This enhances its interaction with the excitonic dipole, and hence reduces the required external power constituting the background. Furthermore, using nanophotonic devices, the FWM is efficiently collected by the detection optics, avoiding the total internal reflection affecting planar structures: assuming the gain in the collection efficiency $\eta$ and an $n$-time enhancement of the local excitation intensity, the FWM amplitude is in-

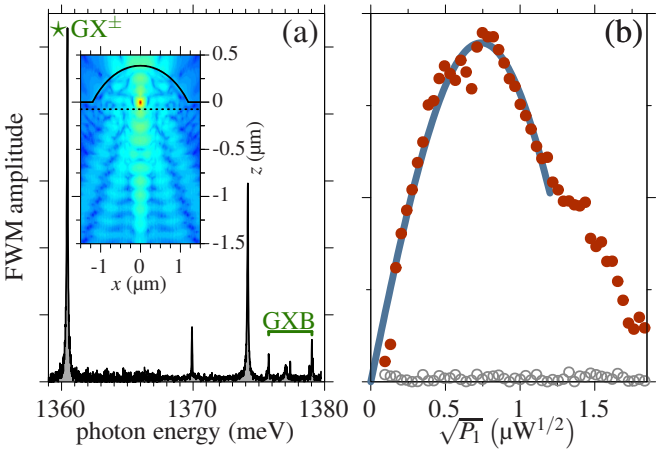


FIG. 1. (a) Spectrally-resolved FWM amplitude generated by a few QD excitons embedded in a lens structure. The targeted QD trion ($GX^{\pm}$) is labeled with the green $\star$. The horizontal bar indicates a neutral exciton-biexciton system (GXB) in a QD located at the lens periphery. Inset: Calculated distribution of the near-field intensity for the QD-lens structure. The semiconductor-air interface is shown by the solid black line and the DBR starts below the dashed line. (b) Spectrally-integrated FWM amplitude of a trion in the target QD as a function of the pulse area $\theta_1 \propto \sqrt{P_1}$ of $\mathcal{E}_1$. The blue line shows the fit to the expected $|\sin(\theta_1/2)|$ amplitude dependence of the FWM.

creased by $\sqrt{\eta n^3}$, while maintaining the external power of exciting laser pulses $\mathcal{E}_{1,2,3}$.

In contrast to the previous work, the EBL overcomes the issue of a low yield of optimally functioning devices, when patterning the sample containing randomly distributed QDs. Microlenses processed with EBL can be defined deterministically, spatially matched to QDs with about 30 nm alignment accuracy [21], combined with frequency matching guaranteed by their broadband operation beyond 100 nm.

Microlenses with a height of 0.35 µm and 2 µm diameter have been etched, as described in detail in Ref. [9], so as to create the hot spot of the excitation and detection mode field exactly at the QD plane, located between the underneath Bragg reflector and the microlens surface [8] - see inset in Figure 1 a. We use InAs QDs grown by metalorganic chemical vapor deposition [23]. As a result of the high light-extraction efficiency [22] of around 30 % in our devices, we routinely note a bright QD photoluminescence, with spectrally-integrated count rate of 200 kHz below the PL saturation (not shown). For comparison, up to 1 kHz PL count rates are typically observed in our setup for high quality QDs embedded in planar samples.

For the FWM spectroscopy we use radio-frequency acousto-optic deflectors providing frequency shifts of $\Omega_{1,2,3}$ for $\mathcal{E}_{1,2,3}$, respectively. FWM signals are then detected by performing optical heterodyning. To select the required heterodyne beat component, we interfere the reflected field with a frequency shifted reference field $\mathcal{E}_R$. Spectrally-resolved interferograms are recorded by a CCD camera [18, 20] and analyzed by spectral interferometry to retrieve amplitude and phase of the signal. In Fig. 1a we show an exemplary two-pulse FWM spectrum, (driving with $\mathcal{E}_1$ and $\mathcal{E}_2$ and detecting at the heterodyne frequency $2\Omega_2 - \Omega_1$), over a range of 25 meV displaying several excitonic transitions. Owing to a strongly improved excitation and collection compared to planar structures [24], we here achieve a gain in the signal-to-noise ratio of the measured FWM amplitude by two-orders of magnitude. Exciton-biexciton pairs can be identified (an example is denoted with a green bar above 1375 meV) by employing FWM polarization and delay selection rules [25] (not shown). Similar FWM signal was found on another investigated microlens, pointing toward the deterministic character and high-quality of the EBL nano-processing platform.

In the following, we study the dominating transition at 1360.4 meV labeled as $\star$ in Figure 1a. This is to minimize the time required to perform following FWM sequences and thus to avoid drifts. We observe no FWM at $\tau_{12} < 0$, showing that it stems from a charged exciton (trion) transition $GX^{\pm}$ [25]. To illustrate the enhanced in-coupling of $\mathcal{E}_{1,2,3}$ offered by the microlenses, in Figure 1b we present the FWM amplitude as a function of the pulse area $\theta_1 \propto \sqrt{P_1}$, where $P_1$ represents the intensity of $\mathcal{E}_1$, while $P_2$ is fixed to 1.5 µW. The FWM signal displays a Rabi rotation following the expected $|\sin(\theta_1/2)|$ dependence [26] with the first maximum at $\sqrt{P_1} = 0.75\,\mu W^{1/2}$, corresponding to a pulse area of $\theta_1 = \pi/2$. For higher intensities the FWM signal deviates from this behavior.

To measure the exciton density lifetime $T_1$, we employed the three-pulse FWM, where the signal is detected at $\Omega_3 + \Omega_2 - \Omega_1$, as a function of the second delay $\tau_{23}$, displayed in Figure 2. From its exponential decay we determine the lifetime [19, 20] to $T_1 = (347 \pm 12)$ ps at $T = 5$ K. Such a rather short lifetime, compared to about 1 ns typically observed [27] in these structures, is attributed to the selectivity of the FWM technique favoring particularly bright QDs with high dipole moment and thus displaying fast population decay dynamics (less intense transitions in Fig. 1a are expected to exhibit longer $T_1$). Additionally, the radiative lifetime is slightly shortened due to a Purcell effect of the microlenses [9].

We now turn to the measurement of coherence dynamics as a function of temperature, to determine the impact of the phonon-interaction on the exciton dephasing. The FWM transient, generated in our time-averaged and multi-repetition heterodyne experiment, is emitted after the arrival of $\mathcal{E}_2$. It is expected to exhibit a Gaussian echo [19, 24], owing to a Gaussian spectral wandering of standard deviation $\sigma$, with the maximum at $t = \tau_{12}$ and temporal full width at half maximum (FWHM) of $\hbar\sqrt{8\ln(2)}/\sigma$. To retrieve $\sigma$, we apply the pulse sequence depicted in Figure 3a, namely we keep fixed $\tau_{12} = 110$ ps

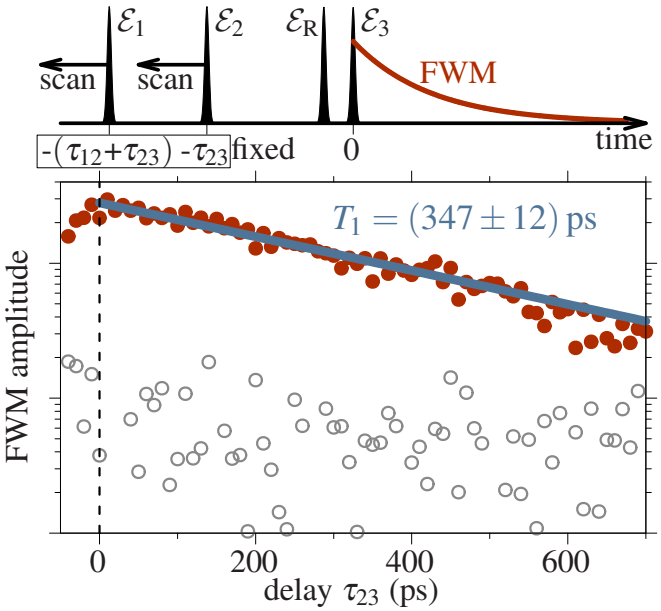


FIG. 2. Top: Three-pulse sequence employed to measure the trion population dynamics. $\mathcal{E}_1$ and $\mathcal{E}_2$, having a delay of $\tau_{12} = 20$ ps, create the trion population and are jointly advanced in time, such that the FWM triggered by $\mathcal{E}_3$ probes the population decay via the $\tau_{23}$ dependence. Bottom: Measurement yielding the exciton lifetime $T_1 = (347 \pm 12)$ ps. The noise level is indicated by open circles.

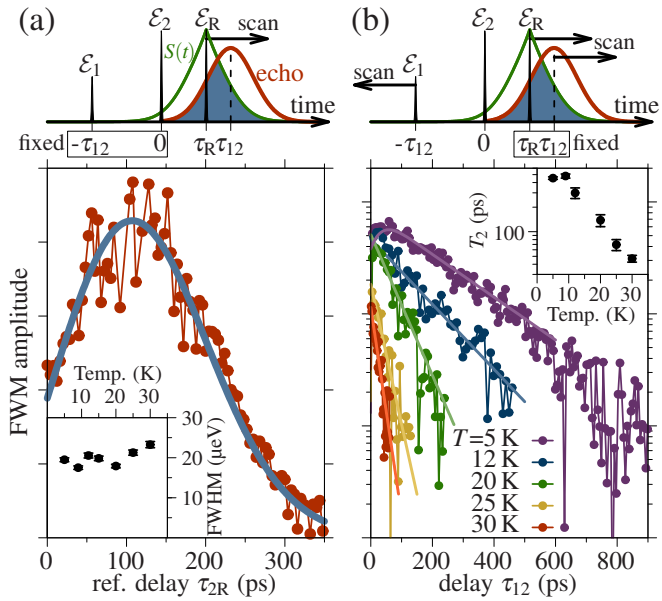


FIG. 3. (a) Top: Two-pulse sequence applied to probe the echo profile. Bottom: Integrated FWM amplitude versus $\tau_{2R}$ at 5 K revealing the Gaussian echo with a temporal width yielding $\sigma$; the theoretical fit is given by the solid line. Inset: Inhomogeneous broadening $\sqrt{8\ln(2)}\sigma$ retrieved from the echo temporal width for different temperatures. (b) Top: Two-pulse sequence applied to probe the trion dephasing. Bottom: Measured FWM amplitude as function of the delay $\tau_{12}$, yielding coherence dynamics for different temperatures; theoretical fits as solid lines. Inset: Dephasing time $T_2$ as a function of temperature.

while scanning the delay $\tau_{2R}$ between $\mathcal{E}_2$ and $\mathcal{E}_R$. As such, the temporal sensitivity of the experiment $S(t)$ (green curve centered around $\mathcal{E}_R$), originating from the finite spectral resolution of the spectrometer, is scanned through a broad FWM transient. A measurement of $S(t)$ is given in the Supporting Information Figure 1S. The FWM integrated overlap between $S(t)$ and the echo plotted against $\tau_{2R}$ in Figure 3a indeed reproduces a Gaussian form, with the expected maximum at $\tau_{12} = 110$ ps and $\sigma = 8.2$ μeV. The measured inhomogeneous broadening (FWHM) $\sqrt{8\ln(2)}\sigma$ is plotted versus temperature in the inset, where we find that it varies only marginally within the investigated temperature range.

To extract the ZPL dephasing rate $\gamma = 1/T_2$ we measure the time-integrated FWM amplitude as a function of $\tau_{12}$. For a fixed $\tau_{2R}$, the echo moves through $S(t)$ when varying $\tau_{12}$. This has previously been compensated by correcting the signal in the time domain by $S(t)$ [19, 20, 24]. However, for sufficiently large $\tau_{12}$, the echo is generated at times not accessible via $S(t)$, such that the signal cannot be retrieved via spectral interference. Here, this issue is overcome by simultaneously increasing $\tau_{2R}$ towards positive times when increasing $\tau_{12}$, such that $S(t)$ probes the same time-portion of the echo for every $\tau_{12}$, as depicted in Figure 3b. We initially set $\tau_{2R} = -70$ ps to assure the time ordering between $\mathcal{E}_R$ and FWM, as required to perform spectral interferometry. The resulting FWM amplitude for several temperatures is presented in Figure 3b.

After the echo has developed for $\tau_{12} > 150$ ps, the decay of the signal is given by a single exponential, yielding the dephasing time $T_2$. At low temperature the latter reaches $T_2 \approx 1.3T_1$, close to the radiative limit ($T_2 = 2T_1$), in spite of the significant inhomogeneous broadening. As shown in the inset, with increasing temperature, $T_2$ shortens rapidly consistently with previous measurements on ensembles [12] and more recent complementary approaches employing photon-correlation techniques [27]. The dominant term in the electron-phonon coupling in semiconductors is linear in the lattice displacement, i.e., it is linear in the phonon creation and annihilation operators. For the present case of a QD excited at the lowest exciton transition, which represents a two-level system, this reduces to the independent boson model [15]. This model, for the 3D acoustic phonon density of states, provides a band of phonon assisted transitions and an unbroadened ZPL. The finite width of the ZPL and its temperature dependence are explained by phonon processes, which are of second order in the phonon operators that may originate from virtual transitions to higher excitonic states [16] or phonon anharmonicities [17], which are not included in our model.

Figure 3b also reveals a pronounced decrease of the ini-

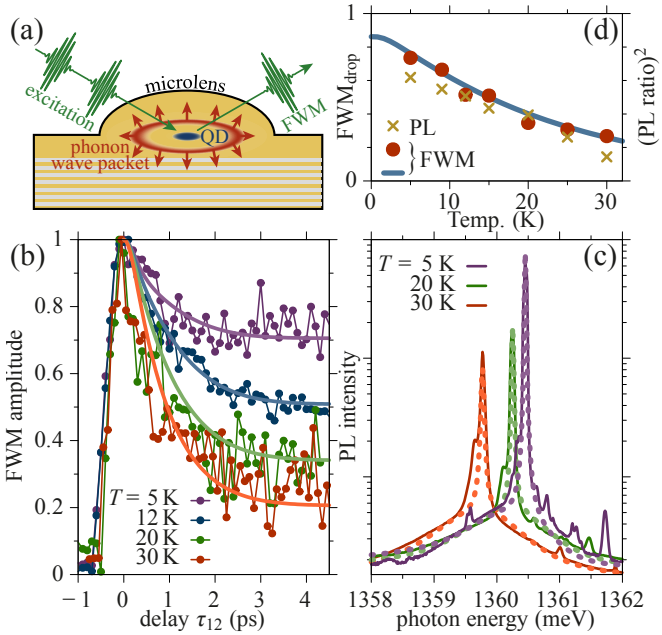


FIG. 4. (a) Cartoon depicting propagation of a phonon packet from a QD after its excitation with a short, femto-second pulse. (b) Two-pulse time-integrated FWM amplitudes for initial delays $\tau_{12}$. The FWM amplitudes at different temperatures (see legend) are normalized at $\tau_{12} = 0$ to show the phonon-induced dephasing. (c) PL spectra for different temperatures. Solid lines: experimental data; dashed lines: theoretical curves. (d) Final FWM values after the initial decay (red cirles) as function of temperature along with the theoretical calculation (blue line) (cf. panel b). Additional temperatures for b) and c) are shown in the Supporting Information Figure 2S. $Z^2$ estimated from temperature dependent PL spectra are given by gold crosses.

tial FWM amplitude at $\tau_{12} = 0$ with increasing temperature, such that the signal cannot be measured beyond $T = 35\,\mathrm{K}$. This rapid initial decrease is attributed to the phonon-induced dephasing caused by the linear coupling to phonons, which dominates the short-time behavior of the signal. To analyze this effect we measure the coherence dynamics on a picosecond time scale. The results are shown in Figure 4. The linear coupling describes the fact that the equilibrium positions of the lattice ions in the presence of an exciton are different from their values in the absence of an exciton, i.e., a polaron is formed. When an exciton is abruptly generated by a femto-second pulse, the quick formation of the polaron is accompanied by the emission of a phonon wave packet [14, 28], traveling through the QD volume and then through the surrounding lattice with the sound velocity of about 5 nm/ps, as illustrated in Figure 4a. Once the wavepacket has left the QD, the phonon-assisted transitions have dephased and are not further contributing to the FWM. In the $\tau_{12}$-dependence of the FWM signal this manifests itself as a fast decay on a timescale of about 2 ps [29] clearly revealed in Figure 4b.

The final value after the initial drop $\mathrm{FWM_{drop}}$ is plotted as a function of temperature in Figure 4d. With increasing temperature the phonon coupling becomes more effective and, accordingly, already at $T = 30\,\mathrm{K}$ the coherence decays by a factor of 5 during the first 5 ps. This explains why the initial value of the signal seen in Figure 3b, where this initial decay is not resolved, rapidly decays with increasing temperatures.

In the spectral domain, the initial decay is associated with a broad phonon background around a zero-phonon line (ZPL) [29, 30]. This is seen in the photoluminescence (PL) spectra taken from the same QD, shown in Figure 4c. For low temperatures the background is asymmetric reflecting the dominance of phonon emission processes over absorption processes, while at higher temperatures, when the thermal occupation of the involved phonons becomes much larger than one, the phonon background becomes symmetric.

For the theoretical modeling of the signals we employ the standard model of a QD coupled to acoustic phonons via the pure dephasing mechanism [10, 11, 29–31], which has been proven to successfully describe a variety of optical phenomena in single QDs and QD ensembles. For this model exact analytical formulas for linear and nonlinear optical signals after excitation with an arbitrary series of short laser pulses can be obtained within a generating function formalism [32, 33]. To be specific, we model the QD trion transition as a two-level system, which is coupled via deformation potential coupling to longitudinal acoustic (LA) phonons with a linear dispersion relation. Assuming an approximately harmonic confinement potential, we take Gaussian-shaped wave functions for electrons and holes with electron localization lengths $a_r$ in the in-plane direction and $a_z$ in the out-of-plane direction, i.e., we model a lens-shaped QD and treat the exciton wave function as a product of electron and hole wave functions.

The results of our calculations are shown as solid lines in Figure 4b and as dashed lines in Figure 4c. We use electron localization lengths $a_r = 8\,\mathrm{nm}$ and $a_z = 1\,\mathrm{nm}$ (the respective hole localization lengths are scaled by 0.87) and assume GaAs parameters. We find an excellent agreement between theory and experiment for both the FWM signals and the PL spectra over the whole range of temperatures, however for an increased phonon coupling strength. Specifically, to achieve agreement with both the FWM signal and phonon background in PL simultaneously, we had to increase the phonon coupling constant by a factor of 1.5. This we model by increased deformation potentials $D^{\mathrm{e}} = 10.5\,\mathrm{eV}$ and $D^{\mathrm{h}} = -5.25\,\mathrm{eV}$, with respect to the standard parameters $D^{\mathrm{e}} = 7.0\,\mathrm{eV}$ and $D^{\mathrm{h}} = -3.5\,\mathrm{eV}$, which have previously been used to quantitatively describe various optical signals from QD structures [10, 34, 35]. A more detailed discussion of the role of the parameters for the FWM signals and PL spectra can be found in the Supplemental Information. While we

do not have a definite explanation, we note that similarly higher values for the deformation potentials can also be found in the literature [36], and an increased deformation potential has also been used to explain mobilities in a 2DEG [37–39]. One explanation could be that in the present sample there are additional mechanisms like piezo-electric coupling, which are usually negligible but contribute here, e.g., because of an increased spatial separation of electron and hole wave functions [28], leading to an effective increase of the coupling described by larger deformation potentials.

Finally, it is instructive to compare FWM initial decay with the ZPL weight in PL [12] ($Z$), defined as fraction of ZPL in the total absorption spectrum. Within the formalism describing our experiment we obtain $\mathrm{FWM}_{\mathrm{drop}} \propto Z^2$. We approximate $Z$ as the PL ratio between the measured ZPL and the entire PL, including the phonon background. In spite of finite spectral resolution and significant $\sigma$, for all considered temperatures we obtain close agreement between $\mathrm{FWM}_{\mathrm{drop}}$ and $Z^2$ independently estimated from PL, as shown in Figure 4d.

In this Article, we have employed EBL to deterministically embed QDs within microlenses, providing a convenient nanophotonic platform to perform coherent nonlinear spectroscopy of individual QDs. Microlens structures enabled to efficiently penetrate across the dielectric boundary and to tightly focus the light field around the QD, which has been exploited to perform FWM microspectroscopy. We have measured and modeled the role of acoustic phonons on the coherence of single QD excitons, in particular corroborating signatures of single phonon wave packet emission in FWM and PL. Our fundamental studies, aiming to understand the complex interplay between charges and lattice vibrations, are at the heart of condensed matter optics. They are relevant for a large class of individual emitters in solids, like epitaxial and colloidal QDs or colour centres in diamond, or emerging QD-like emitters in transition-metal dichalcogenides [40–42]. Our findings are also pertinent for ultrafast nonlinear nanophotonics, opto-mechanics and phonon transport in nanostructured devices.

*We acknowledge the financial support by the European Research Council (ERC) Starting Grant PICSEN (grant no. 306387) and the German Research Foundation (DFG) within the Collaborative Research Center SFB 787, the German Federal Ministry of Education and Research (BMBF) through the VIP-project QSOURCE (Grant No. 03V0630), and by the project EMPIR 14IND05 MIQC2 within the European Union's Horizon 2020 research and innovation programme.*

* tomasz.jakubczyk@neel.cnrs.fr
† d.wigger@wwu.de
‡ stephan.reitzenstein@physik.tu-berlin.de
§ jacek.kasprzak@neel.cnrs.fr

[1] Borri, P.; Langbein, W.; Schneider, S.; Woggon, U.; Sellin, R. L.; Ouyang, D.; Bimberg, D. Ultralong dephasing time in InGaAs quantum dots. *Phys. Rev. Lett.* **2001**, *87*, 157401.

[2] Curto, A. G.; Volpe, G.; Taminiau, T. H.; Kreuzer, M. P.; Quidant, R.; van Hulst, N. F. Unidirectional emission of a quantum dot coupled to a nanoantenna. *Science* **2010**, *329*, 930.

[3] Ma, Y.; Ballesteros, G.; Zając, J. M.; Sun, J.; Gerardot, B.D. Highly directional emission from a quantum emitter embedded in a hemispherical cavity. *Optics Lett.* **2015**, *40*, 2373.

[4] Claudon, J.; Bleuse, J.; Malik, N. S.; Bazin, M.; Jaffrennou, P.; Gregersen, N.; Sauvan, C.; Lalanne, P.; Gérard, J.-M. A highly efficient single-photon source based on a quantum dot in a photonic nanowire. *Nature Photon.* **2010**, *4*, 174.

[5] Ding, X.; He, Y.; Duan, Z.-C.; Gregersen, N.; Chen, M.-C.; Unsleber, S.; Maier, S.; Schneider, C.; Kamp, M.; Höfling, S.; Lu, C.-Y.; Pan, J.-W. On-demand single photons with high extraction efficiency and near-unity indistinguishability from a resonantly driven quantum dot in a micropillar. *Phys. Rev. Lett.* **2016**, *116*, 020401.

[6] Donatini, F.; Dang, L. S. Electronic lithography method with cathodoluminescence imaging. *WO Patent App. PCT/FR2010/00,226* **2010**,

[7] Donatini, F.; Dang, L. S. A single-step electron beam lithography of buried nanostructures using cathodoluminescence imaging and low temperature. *Nanotechnology* **2010**, *21*, 375303.

[8] Gschrey, M.; Thoma, A.; Schnauber, P.; Seifried, M.; Schmidt, R.; Wohlfeil, B.; Krüger, L.; Schulze, J.-H.; Heindel, T.; Burger, S.; Strittmatter, A.; Rodt, S.; Reitzenstein, S. Highly indistinguishable photons from deterministic quantum-dot microlenses utilizing three-dimensional in situ electron-beam lithography. *Nature Comm.* **2015**, *6*, 7662.

[9] Kaganskiy, A.; Gschrey, M.; Schlehahn, A.; Schmidt, R.; Schulze, J.-H.; Heindel, T.; Strittmatter, A.; Rodt, S.; Reitzenstein, S. Advanced in-situ electron-beam lithography for deterministic nanophotonic device processing. *Rev. Sci. Instrum.* **2015**, *86*, 073903.

[10] Reiter, D. E.; Kuhn, T.; Glässl, M.; Axt, V. M. The role of phonons for exciton and biexciton generation in an optically driven quantum dot. *J. Phys. Condens. Matter* **2014**, *26*, 423203.

[11] Ramsay, A. J. A review of the coherent optical control of the exciton and spin states of semiconductor quantum dots. *Semicond. Sci. Technol.* **2010**, *25*, 103001.

[12] Borri, P.; Langbein, W.; Woggon, U.; Stavarache, V.; Reuter, D.; Wieck, A. D. Exciton dephasing via phonon interactions in InAs quantum dots: Dependence on quantum confinement. *Phys. Rev.* B **2005**, *71*, 115328.

[13] Krügel, A.; Vagov, A.; Axt, V. M.; Kuhn, T. Monitoring the buildup of the quantum dot polaron: Pump-probe and four-wave mixing spectra from excitons and biexcitons in semiconductor quantum dots. *Phys. Rev.* B **2007**, *76*, 195302.

[14] Wigger, D.; Lüker, S.; Reiter, D. E.; Axt, V. M.; Machnikowski, P.; Kuhn, T. Energy transport and coherence properties of acoustic phonons generated by optical excitation of a quantum dot. *J. Phys. Condens. Matter* **2014**,

*26*, 355802.

[15] Mahan, G.D. Many-Particle Physics (Kluwer, New York, 2000).

[16] Muljarov, E. A.; Zimmermann, R. Dephasing in quantum dots: Quadratic coupling to acoustic phonons. *Phys. Rev. Lett.* **2004**, *93*, 237401.

[17] Machnikowski, P. Change of Decoherence Scenario and Appearance of Localization due to Reservoir Anharmonicity. *Phys. Rev. Lett.* **2006**, *96*, 140405.

[18] Langbein, W.; Patton, B. Heterodyne spectral interferometry for multidimensional nonlinear spectroscopy of individual quantum systems. *Opt. Lett.* **2006**, *31*, 1151.

[19] Mermillod, Q.; Jakubczyk, T.; Delmonte, V.; Delga, A.; Peinke, E.; Gérard, J.-M.; Claudon, J.; Kasprzak, J. Harvesting, Coupling, and Control of Single-Exciton Coherences in Photonic Waveguide Antennas. *Phys. Rev. Lett.* **2016**, *116*, 163903.

[20] Fras, F.; Mermillod, Q.; Nogues, G.; Hoarau, C.; Schneider, C.; Kamp, M.; Höfling, S.; Langbein, W.; Kasprzak, J. Multi-wave coherent control of a solid-state single emitter. *Nature Photon.* **2016**, *10*, 155.

[21] Gschrey, M.; Schmidt, R.; Schulze, J.-H.; Strittmatter, A.; Rodt, S.; Reitzenstein, S. Resolution and alignment accuracy of low-temperature in situ electron beam lithography for nanophotonic device fabrication. *J. Vac. Sci. Technol. B* **2015**, *33*, 021603.

[22] Schlehahn, A.; Schmidt, R.; Hopfmann, C.; Schulze, J.-H.; Strittmatter, A.; Heindel, T.; Gantz, L.; Schmidgall, E. R.; Gershoni, D.; Reitzenstein, S. Generating single photons at gigahertz modulation-speed using electrically controlled quantum dot microlenses. *Appl. Phys. Lett.* **2016**, *108*, 021104.

[23] Prohl, Ch.; Lenz, A.; Roy, D.; Schuppang, J.; Stracke, G.; Strittmatter, A.; Pohl, U.W.; Bimberg, D.; Eisele, H.; Dähne, M. Spatial structure of $In_{0.25}Ga_{0.75}As/GaAs/GaP$ quantum dots on the atomic scale. *Appl. Phys. Lett.* **2013**, *102*, 123102.

[24] Kasprzak, J.; Portolan, S.; Rastelli, A.; Wang, L.; Plumhof, J. D.; Schmidt, O. G.; Langbein, W. Vectorial nonlinear coherent response of a strongly confined exciton–biexciton system. *New J. Phys.* **2013**, *15*, 055006.

[25] Mermillod, Q.; Wigger, D.; Delmonte, V.; Reiter, D. E.; Schneider, C.; Kamp, M.; Höfling, S.; Langbein, W.; Kuhn, T.; Nogues, G.; Kasprzak, J. Dynamics of excitons in individual InAs quantum dots revealed in four-wave mixing spectroscopy. *Optica* **2016**, *3*, 377.

[26] Patton, B.; Woggon, U.; Langbein, W. Coherent control and polarization readout of individual excitonic states. *Phys. Rev. Lett.* **2005**, *95*, 266401.

[27] Thoma, A.; Schnauber, P.; Gschrey, M.; Seifried, M.; Wolters, J.; Schulze, J.-H.; Strittmatter, A.; Rodt, S.; Carmele, A.; Knorr, A.; Heindel, T.; Reitzenstein, S. Exploring dephasing of a solid-state quantum emitter via time-and temperature-dependent Hong-Ou-Mandel experiments. *Phys. Rev. Lett.* **2016**, *116*, 033601.

[28] Krummheuer, B.; Axt, V. M.; Kuhn, T.; D'Amico, I.; Rossi, F. Pure dephasing and phonon dynamics in GaAs- and GaN-based quantum dot structures: Interplay between material parameters and geometry. *Phys. Rev.* B **2005**, *71*, 235329.

[29] Krummheuer, B.; Axt, V. M.; Kuhn, T. Theory of pure dephasing and the resulting absorption line shape in semiconductor quantum dots. *Phys. Rev.* B **2002**, *65*, 195313.

[30] Besombes, L.; Kheng, K.; Marsal, L.; Mariette, H. Acoustic phonon broadening mechanism in single quantum dot emission. *Phys. Rev.* B **2001**, *63*, 155307.

[31] Förstner, J.; Weber, C.; Danckwerts, J.; Knorr, A. Phonon-Assisted Damping of Rabi Oscillations in Semiconductor Quantum Dots. *Phys. Rev. Lett.* **2003**, *91*, 127401.

[32] Vagov, A.; Axt, V. M.; Kuhn, T. Electron-phonon dynamics in optically excited quantum dots: Exact solution for multiple ultrashort laser pulses. *Phys. Rev.* B **2002**, *66*, 165312.

[33] Axt, V. M.; Kuhn, T.; Vagov, A.; Peeters, F. M. Phonon-induced pure dephasing in exciton-biexciton quantum dot systems driven by ultrafast laser pulse sequences. *Phys. Rev.* B **2005**, *72*, 125309.

[34] Vagov, A.; Axt, V. M.; Kuhn, T.; Langbein, W.; Borri, P.; Woggon, U. Nonmonotonous temperature dependence of the initial decoherence in quantum dots. *Phys. Rev.* B **2004**, *70*, 201305.

[35] Quilter, J. H.; Brash, A. J.; Liu, F.; Glässl, M.; Barth, A. M.; Axt, V. M.; Ramsay, A. J.; Skolnick, M. S.; Fox, A. M. Phonon-assisted population inversion of a single InGaAs/GaAs quantum dot by pulsed laser excitation. *Phys. Rev. Lett.* **2015**, *114*, 137401.

[36] Adachi, S. *Physical properties of III-V semiconductor compounds*; John Wiley & Sons, 1992.

[37] Gorczyca, I.; Suski, T.; Litwin-Staszewska, E.; Dmowski, L.; Krupski, J.; Etienne, B. Deformation potential in a high-electron-mobility $GaAs/Ga_{0.7}Al_{0.3}As$ heterostructure: Hydrostatic-pressure studies. *Phys. Rev.* B **1992**, *46*, 4328.

[38] Kawamura, T.; Das Sarma, S. Temperature dependence of the low-temperature mobility in ultrapure $Al_xGa_{1-x}As/GaAs$ heterojunctions: Acoustic-phonon scattering. *Phys. Rev.* B **1990**, *42*, 3725.

[39] Scholz, R. Hole–phonon scattering rates in gallium arsenide. *J. Appl. Phys.* **1995**, *77*, 3219.

[40] Kern, J.; Niehues, I.; Tonndorf, P.; Schmidt, R.; Wigger, D.; Schneider, R.; Stiehm, T.; Michaelis de Vasconcellos, S.; Reiter, D. E.; Kuhn, T.; Bratschitsch, R. Nanoscale Positioning of Single-Photon Emitters in Atomically Thin WSe2. *Adv. Mater.* **2016**, *28*, 7101.

[41] Kumar, S.; Brotóns-Gisbert, M.; Al-Khuzheyri, R.; Branny, A.; Ballesteros-Garcia, G.; Sánchez-Royo, J. F.; Gerardot, B. D. Resonant laser spectroscopy of localized excitons in monolayer WSe 2. *Optica* **2016**, *3*, 882.

[42] He, Y.-M.; Höfling, S.; Schneider, C. Phonon induced line broadening and population of the dark exciton in a deeply trapped localized emitter in monolayer $WSe_2$. *Optics express* **2016**, *24*, 8066.